ACCSCIENCE PUBLISHING

International Journal of Bioprinting

RESEARCH ARTICLE

Mimicking human skin constructs using norbornene-pullulan-based hydrogels

Angela Cirulli[1], Livia Neves Borgheti-Cardoso[1], Núria Torras[1]*, and Elena Martínez[1,2,3]*

[1]Biomimetic Systems for Cell Engineering Laboratory, Institute for Bioengineering of Catalonia, The Barcelona Institute of Science and Technology, Barcelona, Spain

[2]Centro de Investigación Biomédica en Red, Madrid, Spain

[3]Department of Electronics and Biomedical Engineering, University of Barcelona, Barcelona, Spain

Abstract

There has been a huge demand for engineered skin tissues in the realms of both *in vitro* and *in vivo* applications. Selecting the right material scaffold is a critical consideration in making engineered skin tissues, since it should possess a good balance between elasticity and mechanical stability while promoting an adequate cell microenvironment to support both the dermal and the epidermal compartments of skin tissue. In this study, 3D-bioprinted norbornene-pullulan photocrosslinkable hydrogels were utilized as alternative scaffolds to produce epithelized dermal skin models. By employing visible light, 2.5 mm^3 cell-laden hydrogels could be printed in 10 s. The thiol-ene photocrosslinking chemistry employed in this work enabled the formation of a well-defined extracellular matrix with orthogonal crosslinks, where encapsulated fibroblasts maintained high cellular viability rates. Through this method, an epidermal layer could be grown on top of the fibroblasts. The coexistence and interaction of human fibroblasts and keratinocytes were visualized by determining the expression of specific markers. This approach represents a promising starting point for the development of photocrosslinkable hydrogel-based human skin constructs by using thiol-ene norbornene chemistry, paving the way toward manufacture of complex *in vitro* models of human tissues.

Keywords: Skin models; Photocrosslinkable hydrogels; Pullulan; Light-based 3D bioprinting

***Corresponding authors:**
Núria Torras (ntorras@ibecbarcelona.eu)

Elena Martínez (emartinez@ibecbarcelona.eu)

Citation: Cirulli A, Borgheti-Cardoso LN, Torras N, Martínez E. Mimicking human skin constructs using norbornene-pullulan-based hydrogels. *Int J Bioprint*. 2024;10(4):3395. doi: 10.36922/ijb.3395

Received: April 9, 2024
Accepted: May 24, 2024
Published Online: July 3, 2024

1. Introduction

The skin structure can be organized into three major layers, namely hypodermis, dermis, and epidermis, with each of the layers providing different mechanical properties depending on its cellular composition and type of structure.[1] Engineered skin tissues can be employed in clinical applications, including skin substitution and advanced wound dressing, as well as in the pre-clinical scenarios to facilitate drug absorption, disease modeling, and cosmetic studies. An ideal engineered skin tissue should be easy to prepare, resistant mechanical shear forces, and suitable for cells to adhere, grow, and vascularize, in both epidermal and dermal compartments.[2,3]

Collagen represents the gold-standard biomaterial for the fabrication of skin surrogates since it is the main structural protein found in connective tissues, including the skin,[4] and the most abundant protein in the extracellular matrix.[5,6] Usually, collagen is derived from raw materials such as bovine and porcine tissues,[7] possessing good flexibility, as well as thermal and enzymatic stability. Different collagen-based models have been developed as *in vitro* systems, including a model for irritation testing.[8] *In vivo* clinical skin equivalents built with collagen have also garnered considerable interest. An example is FortiCell Bioscience, designed by Orcel®, which integrates human epidermal keratinocytes and dermal fibroblasts cultured on a type I bovine collagen substrate. This innovative formulation is specifically tailored to address the complexities of wound healing in limb afflictions, notably skin ulcers and diabetic conditions. However, it is not exempt from drawbacks. It has been observed that natural collagen is fraught with a perennial problem of batch-to-batch variability, which is not easy to address. It also may produce pathogenic adverse reactions, evidenced by the side effects of bovine collagen implants identified in a small percentage of treated patients.[9,10] In addition, collagen scaffolds tend to collapse under traction forces, especially when the cells are embedded, thus compromising the mechanical stability of the constructs.[11] While culturing, fibroblasts may contract collagen-based hydrogels, causing the loss of close connection between the epidermal layer and the corresponding cell culture support, leading to the loss of skin barrier function.[12] Hence, some reinforcements are necessary to improve the mechanical properties and to reinforce the gel, as reported in a study by Bacakova et al.[11] where a nanofibrous poly-L-lactide (PLLA) membrane was used.

In this context, artificial, recombinant, and synthetic collagens are becoming new options.[13] Also, alternative biomaterials are being considered. Owing to their hydrophilic nature and variable degree of swelling, hydrogels has a better capability in mimicking natural soft tissue than any other types of polymeric biomaterials, proving good biocompatibility, and thus, resulting in attractive scaffolds for cell encapsulation.[14] Gelatin, which is a natural polymer obtained after hydrolysis and denaturation of collagen, has been used as wound dressing mostly in the form of gelatin methacrylate (GelMA), which allows light-based chemical crosslinking of the chains, adding further mechanical stability than just physical crosslinking.[15] Methacrylate kappa-carrageenan (kCA) hydrogels, based on kCA, a natural linear water-soluble polysaccharide, have also been employed for this purpose since kCA resembles natural glycosaminoglycan structure, supplying physical and chemical properties similar to those in native human skin.[16] Hyaluronic acid (HA), which is a non-sulfated glycosaminoglycan, can also be viewed as an alternative. It participates in several crucial functions *in vivo*, such as tissue hydrodynamics and regulation in wound healing processes, generating networks that are suitable for cell growth and migration, thereby promoting angiogenesis.[17,18] For *in vitro* applications, synthetic polymers are regarded as excellent alternatives due to their non-degradability, reproducibility, and ability to endure long-term studies, as in the case of polyethylene glycol (PEG) and polyvinyl alcohol (PVA). However, some limitations also occur when they are used alone, such as insufficient elasticity. Thus, they could also be blended with natural polymers to develop new materials with enhanced properties, specifically for applications in wound healing.[19] Pullulan (PLN), a water-soluble microbial polysaccharide, is an emerging biopolymer with a set of advantageous properties: it is non-immunogenic, non-toxic, non-carcinogenic, non-mutagenic, and hemocompatible.[20,21] It is also a water-soluble, environmentally friendly polymer. PLN can be crosslinked forming hydrogels with excellent mechanical properties such as tensile strength and modulus, which are attractive for several biomedical and engineering applications, including the production of skin surrogates. To this end, it has been employed together with gelatin to create dermal substitutes both for *in vitro* and *in vivo* testings.[22]

To produce tissue-engineered constructs, one popular approach is the use of three-dimensional (3D) extrusion bioprinting techniques.[23] However, despite the uncontested usefulness, obtaining bioinks with shear thinning properties and addressing the nozzle clogging issues triggered by bioinks still impose some limitations.[24] As an alternative, light-based systems have recently gained popularity for the fabrication of tissue constructs, offering improved spatial resolution, pattern fidelity, and increased fabrication speed.[25,26] These systems involve a light source, typically ultraviolet (UV) or visible light, and low-energy dosages that minimize cell toxicity. A pre-gel solution containing a photoinitiator and eventually a cell suspension is then crosslinked upon illumination. By including a light-patterning feature, modulating the printing parameters, and selecting the proper photopolymerizable materials, 3D cell-laden scaffolds with high cell viability can be produced.[27]

In this study, a novel photocrosslinkable bioink suitable for the engineering of human skin constructs is presented. This bioink capitalizes upon the excellent properties of PLN, which was further functionalized with norbornene groups to form hydrogels upon thiol-norbornene photopolymerization.[19] Upon visible light irradiation, in the presence of a photoinitiator, PLN hydrogels were then formed through a thiol-ene click reaction. Compared to

commonly used radical-mediated polymerization, the thiol-ene click reaction is faster, employs less photoinitiator concentrations, and is not inhibited by oxygen, resulting in hydrogel network with a highly ordered structure.[28–30] Here, norbornene-pullulan (N-PLN) formulations combined with different crosslinkers were successfully employed as a bioink in a customized direct laser writing (DLW) set-up to produce epithelized dermal skin constructs. The dermal compartment was created through the photocrosslinking of a pre-gel solution containing human fibroblasts, while the epidermal compartment was developed by seeding human keratinocytes on top of the fibroblast-laden hydrogels. As shown in this study, fibroblasts could survive, elongate, and spread within the N-PLN matrix up to 24 days post-encapsulation, without showing matrix contraction or collapse due to the cells' presence. Immunostaining studies revealed the expression of basement membrane proteins and keratinocyte surface colonization, consistently characteristic of an epidermal compartment, thus indicating the successful recapitulation of a skin-like structure. This approach, combining visible-light photopolymerization and N-PLN -based materials, presents a promising method for the fabrication of human skin constructs, which is readily employable in *in vitro* drug evaluation for pharmacological and toxicological testing.

2. Materials and methods

2.1. Materials

N-PLN, RGD-modified N-PLN (RGD-N-PLN), thiol-modified polyethylene glycol (PEG-link; 3-D Life PEG Link, L50-1), and thiolated HA modified with a matrix metalloproteinase (MMP)-cleavable peptide (HA-MMP-link) were obtained from Cellendes GmbH, Germany. The HA-MMP-link lyophilisate was dissolved in Milli-Q water to obtain a concentration of 10 mmol/L thiol groups. The freshly dissolved lyophilisate was gently vortexed and incubated for 1–2 h on ice (while shaking occasionally) or at 4°C overnight, followed by an additional gentle mixing. RGD-N-PLN was provided in a solution containing 2.8 mmol/L RGD peptide and 10 mmol/L norbornene groups. A conjugation buffer (3D-Life 10× CB Buffer, pH 7.2; B20-3, Cellendes GmbH, Germany) was also included in the formulation with RGD-N-PLN. Lithium phenyl (2, 4, 6-trimethyl- benzoyl) phosphinate (LAP) (TCI Chemicals) was used as a photoinitiator.

2.2. Preparation of norbornene-pullulan pre-gel solutions

Two different pre-gel solutions based on N-PLN were prepared: (i) N-PLN in combination with a thiol-conjugated PEG-link (*Formulation 1*, containing N-PLN, PEG-link, and LAP), and (ii) RGD-N-PLN in combination with HA-based linker, HA-MMP-link (*Formulation 2*, containing RGD-N-PLN, HA-MMP-link, and LAP). Orthogonal thiol-ene click chemistry was selected as an alternative to the homopolymerization reactions of acrylates or methacrylates for the fabrication of hydrogel-based scaffolds due to its extremely fast photocrosslinking reaction, resulting in homogeneous structures with a high degree of control over the number of reacted functionalities.[31,32] Once it starts, the radical step-growth reaction advances in a stochiometric ratio until the limited moiety (thiol or norbornene) is depleted or unavailable (Figure 1a). As a result, the gelation can be achieved within seconds, with a low concentration of photoinitiator or macromer.[31]

To create the scaffold, a pre-gel solution was prepared (~150 µL) by mixing the combination of polymer and crosslinker (*Formulation 1*—N-PLN: PEG-link: LAP = 5 mM: 4 mM: 0.2 mM; and *Formulation 2*—RGD-N-PLN: HA-MMP-link: LAP = 0.92 mM: 2.5 mM: 2.5 mM: 0.5 mM) in MilliQ water, in the presence of LAP

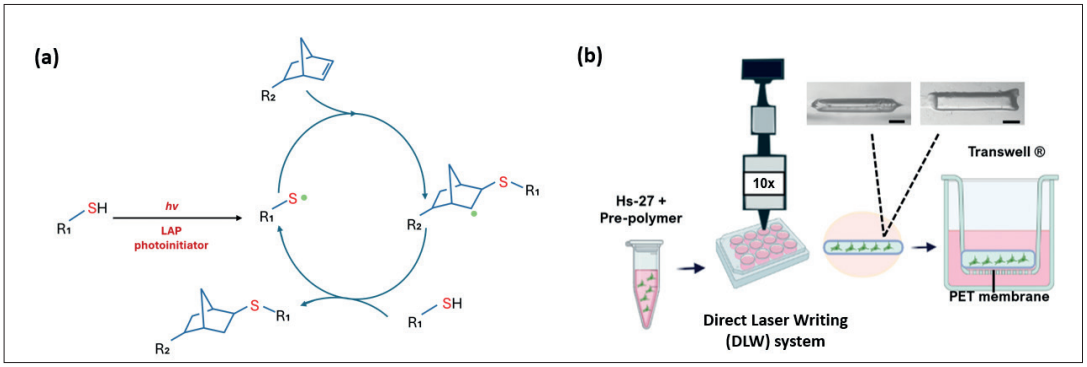

Figure 1. Photopolymerization process of norbornene-based hydrogels. (a) Reaction mechanism of norbornene-based thiol-ene click chemistry. Reprinted with permission of John Wiley and Sons, Copyright © 2024 Wiley Inc.[31] (b) Schematic illustration of hydrogel photopolymerization with Hs-27 encapsulation and consequent mounting within Transwell® inserts. Scale bars = 1 mm.

as a photoinitiator. *Formulation 1* was freshly prepared by dissolving the reagents in MilliQ water at room temperature. In the case of *Formulation 2*, 1× conjugation buffer (CB Buffer) was added. The pre-gel solutions were either photocrosslinked or stored at −20°C until the next use. In the case of cell-laden constructs, a cell suspension of Hs-27 human foreskin fibroblasts (5×10^6 cells/mL) was prepared and mixed with the pre-gel solution right before photocrosslinking (Figure 1b).

2.3. 3D bioprinting system: Direct laser writing

A custom-made 3D bioprinting system based on DLW technique was employed to fabricate the hydrogel-based skin scaffolds. The apparatus is composed of (i) an optical setup consisting of a 405 nm laser diode (DL5146-101S, Thorlabs, NJ, USA), a collimator (LTN330-A, Thorlabs), a lens tube with a HR 10× objective with 0.45 of N/A (Edmund Optics, NJ, USA) coupled to a motorized DC servo actuator (*z*-axis) (Z-series, Thorlabs), and (ii) a motorized translational stage, movable in *x*–*y* plane (Z-series, Thorlabs). All the adaptors and connectors are also from Thorlabs. The system is connected to a personal computer, which enables the control of the writing parameters, such as the speed and acceleration of the translational stage, in both *x* and *y* directions, through LabView software. The laser beam parameters, like the focus and the aperture, can be manually adjusted while the light intensity is regulated by a power supply (LDC200C Series, Thorlabs). Rectangular-shaped hydrogels (5 mm × 1 mm × 0.5 mm) can be crosslinked on a variety of supports, such as well-plates, cover glasses, or PET membranes. For that purpose, the pre-gel solutions were exposed to light at a power ranging from 1 to 41 mW for 10–15 s while the stage was translated in the *x* or *y* directions at a variable speed (0.15–0.30 mm/s). More complex in-plane geometries, for example, grids and circles, can also be printed combining movements of both x and y motors at the same time. The working volume of the hydrogel solutions to be printed was minimized by using circular PDMS pools (6 mm in diameter and 0.5 mm in height), resulting in a 15 µL solution per printed sample, proving the cost-effectiveness of using biopolymers (Figures 1b and S1, Supporting Information). Right after photopolymerization, samples were washed with phosphate-buffered saline (PBS) and kept in submerged conditions at 4°C (without cells) or 37°C (with cells embedded) for later use.

2.4. Mechanical characterization of norbornene-pullulan hydrogels

2.4.1. Volume swelling analysis

To characterize the swelling properties of the hydrogels, pre-gel solutions were irradiated at 405 nm wavelength (Table 1) to photocrosslink hydrogels on top of previously silanized PET membranes. Immediately after photocrosslinking, the samples were washed with PBS to remove non-photocrosslinked residues and carefully wiped with a Kimwipes® tissue (Kim Tech Science). Hydrogels were then kept in PBS at 37°C to induce swelling. Pictures of the hydrogels were taken at different time points with an optical microscope (MZ10 F, Leica, Germany), and the scaffold dimensions were checked and analyzed using ImageJ software. The volumetric swelling ratio was calculated as volume increase due to the swelling (difference between the swollen volume at a certain time "*t*" and the initial volume at time 0) and the initial volume at time 0.

2.4.2. Rheology analysis

For the rheology analysis, hydrogels were fabricated by *in situ* crosslinking within the analysis apparatus. A Discovery HR-2 rheometer equipped with an 8 mm parallel Peltier plate and a UV light source (100–400 nm) (Lightning cure™ LC8 Hamamatsu) was employed for this purpose. Drop volumes of 13 µL of pre-gel solutions were crosslinked with 87.6 mW/cm² power density, measured at the crosslinking plane. The storage (*G*') and loss (*G*") moduli were obtained as a function of the oscillation strain for both pre-gel formulations, by applying a sweep of amplitude between 0.01% and 10³% and keeping constant the frequency to 1 Hz with a fixed running temperature of 25°C. Assuming a Poisson's coefficient value for the soft hydrogels of 0.5,[33] Young's modulus (*E*) was calculated from the values of the complex modulus (*G**), derived from *G*' and *G*" data.

2.5. Fabrication of cell-laden norbornene-pullulan hydrogels

Human foreskin Hs-27 fibroblasts (ATCC-CRL 1634) were used in this study to mimic the dermal compartment of the skin-like constructs. Hs-27 were cultured and expanded in 25 cm² flasks in Dulbecco's Modified Eagle's Medium (DMEM; Gibco, Thermo Fischer Scientific, MA, USA), supplemented with 10% v/v fetal bovine serum (FBS; Gibco, Thermo Fischer Scientific) and 1% v/v penicillin/streptomycin (Sigma-Aldrich, MA, USA). Hs-27 was

Table 1. Printing parameters employed to produce samples for mechanical studies

Polymer formulation	Power (mW)	Stage translational speed (mm/s)
Formulation 1: (N-PLN: PEG-link: LAP)	13	0.3
	22	0.3
	30	0.3
Formulation 2: (RGD-N-PLN: HA-MMP-link: LAP)	22	0.3

incubated at 37°C and 5% CO_2. The culture medium was changed every 2 days, and the cells were passaged twice a week. To fabricate cell-laden scaffolds, Hs-27 cells (5×10^6 cells/mL) were first trypsinized and then resuspended into the freshly prepared pre-gel solutions. For cell culture, hydrogels (5 mm × 1 mm × 0.5 mm) were printed on top of silanized PET membranes of 0.4 μm pore size and 10 mm diameter (it4ip). Then, they were washed with warm cell culture medium supplemented with normocin (1:500; InvivoGen, CA, USA), mounted within Transwell® inserts (Corning®, NY, USA) through double-sided pressure-sensitive adhesive rings,[34] and kept in submerged conditions at 37°C and 5% CO_2. The medium was replaced every 24 h.

2.5.1. Cellular viability

Cell viability assays were conducted on hydrogel scaffolds with Hs-27 embedded at days 1, 3–4, and 7 after the encapsulation, for both formulations, using the calcein-AM/ethidium-homodimer Live/Dead kit (Invitrogen, MA, USA). The gels were incubated with the reagents at 37°C for 20 min, prior to microscopic imaging. During the incubation, the gels were maintained in the 24-well plates covered by aluminum foil, to protect them from light. The cell viability was monitored by a confocal laser scanning microscope (LSM 800, Zeiss, Germany), and the percentage of viable cells was determined manually using ImageJ software (http://imagej.nih.gov/ij, NIH).

2.6. Fabrication and characterization of human skin-like constructs based on norbornene-pullulan hydrogels

2.6.1. Fabrication of 3D human skin-like constructs

Human skin-like constructs were fabricated by seeding HaCaT human keratinocytes (CLS 300493, CLS Cell Lines Service GmbH, Germany), on top of the dermal structure previously generated 3 days after the encapsulation of Hs-27 cells. HaCaT cells were kept in culture in 25 cm^2 flasks in DMEM (Gibco, Thermo Fischer Scientific), supplemented with 10% v/v FBS (Gibco, Thermo Fischer Scientific) and 1% v/v penicillin/streptomycin (Sigma-Aldrich). The cells were kept in incubation at 37°C and 5% CO_2. The medium was changed every 2 days, and the cells were passaged twice a week. To create the co-cultures, HaCaT cells were seeded at a density of 6×10^6 cells/cm^2 on top of fibroblast-laden N-PLN rectangular-shaped hydrogels (5 mm in length, 1 mm in width, and 0.5 mm in height) previously mounted in Transwell® inserts. The cell culture medium employed for the co-cultures was the same used for the maintenance of HaCaT cells added with normocin (1:500; InvivoGen) to prevent contamination, and it was exchanged every 2 days. The co-cultures were maintained for 21 days. For the first 7 days post-HaCaT seeding, all the constructs were kept under submerged conditions, which mean that the culture medium was added both in the basolateral and the apical compartments to fully surround and cover the constructs. Later, ALI culture conditions were applied to some of the scaffolds, by keeping the medium in the basolateral compartment and leaving the apical one exposed to the air.

2.6.2. Immunofluorescence analysis

The cell behavior within the hydrogels and on top of them was characterized by immunostaining. Scaffolds were fixed with 10% neutral buffer formalin solution (Sigma-Aldrich) for 30 min at room temperature in shaking conditions, and then permeabilized with 0.5% Triton-X (Sigma-Aldrich) for 1 h at 4°C. After permeabilization, they were incubated for 2 h at room temperature in shaking conditions, using a blocking buffer solution composed of 1% bovine serum albumin (Sigma-Aldrich), 3% donkey serum (Millipore), and 0.2% Triton-X. For the samples containing only fibroblasts, hydrogels were incubated first with primary antibodies against vimentin (1:100; sc-6260, Santa Cruz, TX, USA), fibronectin (1:200; F3648, Sigma Aldrich, MA, USA), laminin (1:200; ab11575, Abcam, UK), collagen IV (1:250; 134001, Biorad, CA, USA), and Ki67 (1:100; ab16667, Abcam) overnight at 4°C, and then with anti-mouse Alexa Fluor 568, anti-goat Alexa Fluor 647, and anti-rabbit Alexa Fluor 488 (at 4 μg/mL each; Invitrogen, ThermoFisher) as secondary antibodies for 2 h at room temperature. DAPI (Thermo Fisher Scientific) was added to stain the nuclei. For the samples containing fibroblasts and keratinocytes, E-cadherin primary antibody (1:1000; 610181, BD Biosciences, USA) was used to better visualize the HaCaT cells on top of the hydrogels, and keratin 14 primary antibody (1:400; 905301, Biolegend, CA, USA) was used to identify keratin 14, a specifical marker of the basal layer. After incubation, all the samples were flipped down onto a glass coverslip and mounted using a drop of Fluoromount-G® (Southern Biotech, AL, USA) to prevent sample dryness. To avoid sample damage, PDMS spacers (500 μm) were used. Z-stack images were collected using a confocal laser-scanning microscope (LSM 800, Zeiss) and subsequently processed using ImageJ software (http://imagej.nih.gov/ij, NIH).

2.6.3. Transepithelial electrical resistance

To evaluate the integrity of the barrier formed by the keratinocytes on top of the fibroblasts-laden hydrogels, both in submerged and under air-liquid interface (ALI) culturing conditions, the transepithelial electrical resistance (TEER) was monitored for 21 days, starting just before the HaCaT seeding. TEER values were also collected on control samples (HaCaT only cultured on top of hard porous

membranes). In this study, an EVOM3 Epithelial voltmeter with an STX3 electrode (World Precision Instruments, Germany) was employed. Experimental TEER values obtained were corrected by subtracting the resistances due to the hydrogels and the PET membranes and normalized considering the surface area of the hydrogels.

2.7. Statistical analysis

Statistical analysis of data obtained from all the experiments was performed. Data are presented as mean ± standard error of mean (SEM) or standard deviation (SD). The graphs were plotted using GraphPad Prism 8.3.0 software (GraphPad). Experiments for each working condition and formulation were conducted in two to six technical replicates. The Student's *t*-test was employed to analyze the differences in mechanical characterization and level of markers. For cell viability, a two-way analysis of variance (ANOVA) was performed.

3. Results and discussion

3.1. Initial printability tests and physical properties of norbornene-pullulan-based hydrogels

Before the evaluation of the physical characteristics of N-PLN-based formulations, the initial light-induced printability of the two different N-PLN-based formulations (*Formulation 1* and *Formulation 2*) was assessed through DLW, to identify the proper crosslinking molar ratio between the polymer, N-PLN, and the crosslinkers. First, N-PLN: PEG-link: LAP solution (*Formulation 1*) was explored in this respect. Some studies have pointed out that pullulan and PEG are not miscible in certain ratios due to phase separation.[35,36] Upon visible light irradiation, the pre-gel solution containing 5 mM N-PLN, 4 mM PEG-link, and 0.2 mM LAP successfully forms a well-defined crosslinked network, resulting in a shape-retaining scaffold with good consistency and amenability to easy handling. This performance surpasses that of other evaluated molar ratios (5:1, 5:2, 5:3 for N-PLN: PEG-link), when using the same printing parameters (power intensity of 22 mW and a stage translational speed of 0.3 mm/s) (see Figure S2, Supporting Information). This superiority may be attributed to the optimal balance achieved between the functional thiol (SH-) groups present in both the polymer and the linker. As expected, a decrease in the molar ratio between both species correlates with an increase in the crosslinking rate, with the 5:4 ratio yielding the most favorable gelation results.

Later, a hyaluronic acid-based crosslinker (HA-MMP-link) was also examined using RGD-N-PLN: HA-MMP Link: LAP solution (*Formulation 2*). This formulation contains a thiol-modified-HA crosslinker coupled with a matrix metalloproteinase (MMP)-cleavable peptide sequence, which can be cleaved by a broad range of MMPs[37] and allows cells to locally degrade the polymer network if they could produce the indicated MMPs. In the present formulation, the N-PLN polymer was also functionalized with RGD peptide to enhance the scaffold's performance when cells were included.

Initial printability tests showed defined gel geometries using the following molarities for RGD: N-PLN: HA-MMP-link: LAP = 0.92 mM: 2.5 mM: 2.5 mM: 0.5 mM, with a molar ratio of polymer: crosslinker = 1:1, resulting power intensity of 22 mW, and a stage translational speed of 0.3 mm/s, which were the best printing parameters.

Upon determining the optimum molar content (polymer: crosslinker), the impact of printing parameters was evaluated on the gels' properties. The volumetric swelling ratio for *Formulation 1* was first evaluated in samples crosslinked using a power range of 13–30 mW and a stage translational speed of 0.3 mm/s (Table 1). For all the polymerization conditions tested, the equilibrium swelling was reached after 48 hours, showing an overall water uptake capacity of >10%, even though a peak of 27% was reached for one specific crosslinking condition (22 mW, 0.3 mm/s, *Formulation 1*), indicating that this intermediate power may promote the water absorption capability of the network (Figure 2a).

The volumetric swelling behavior for *Formulation 2* was evaluated using samples photocrosslinked with only a power intensity of 22 mW and a stage translational speed of 0.3 mm/s (previously optimized for the specific molar ratio used), also considering the highest uptake capacity registered for *Formulation 1* with these printing parameters. In this case, the equilibrium swelling ratio was ~20%, showing less capacity of these gels to retain water within the scaffold (right column in Figure 2a), compared to *Formulation 1*, and simultaneously suggesting a more compact network.

The swelling is an important parameter to consider since it depends on the crosslinking degree and the porosity, having an impact on the bulk geometry,[38] mass transfer, and therapeutic delivery of substances.[39–41] The greater the extent of crosslinking, the less flexible a hydrogel is to change phase, swell, or shrink, in response to stimuli.[42] Therefore, the choice of materials that exhibit this property is fundamental. It was reported that pure collagen-based gels did not show swelling; in contrast with chemically crosslinked gels such as collagen-HA or thiol-modified HA-based gels.[43]

The bulk mechanical behavior of the two different formulations was also investigated. To this end, rheology measurements were conducted to monitor the crosslinking

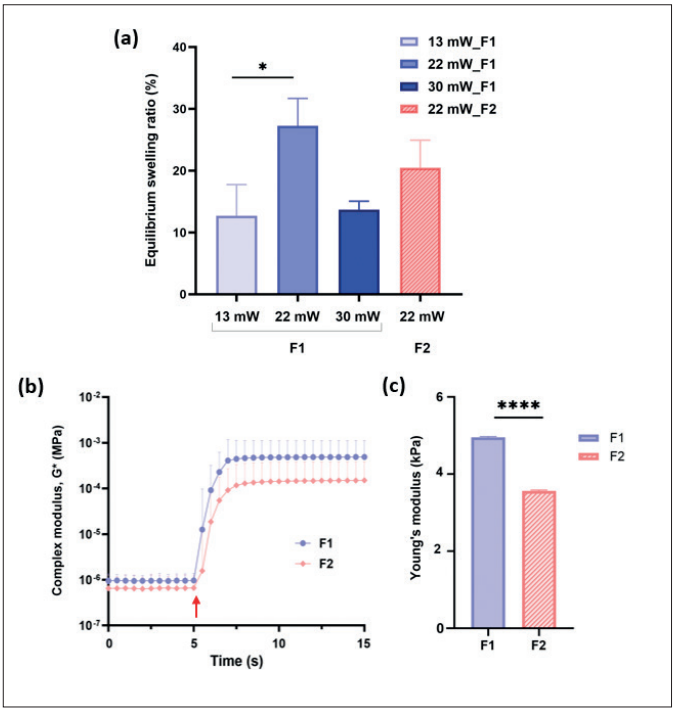

Figure 2. Swelling and mechanical characterization of *Formulation 1* and *Formulation 2*. **(a)** Equilibrium swelling ratios of hydrogels photopolymerized using different working conditions (*Formulation 1*: 13, 22, 30 mW with speed = 0.3 mm/s [$n = 2$ per condition], and *Formulation 2*: 22 mW with speed = 0.3 mm/s [$n = 6$]). **(b)** Complex modulus (G*, MPa) curves registered during the real-time crosslinking process for *Formulation 1* (violet) and *Formulation 2* (pink). The arrow indicates the timepoint when light was switched on. **(c)** Young's modulus values were obtained for *in situ* polymerization tests (*Formulation 1* [violet, $n = 4$], *Formulation 2* [pink, $n = 5$]). In all graphs, values are presented as mean ± SD.

dynamics in real time within the rheometer while exposing the prepolymer solutions to UV light (Figure 2b). When the light is activated, the crosslinking reaction begins and attains a polymerization plateau in under 3 s, evidencing the rapid kinetics of the reaction. Under identical testing conditions, *Formulation 1* yielded a higher complex modulus G* compared to *Formulation 2*, which is translated to statistically significantly higher Young's modulus values (4954 Pa ± 1015 and 3565 Pa ± 1596, respectively; Figure 2c), probably due to the higher N-PLN and PEG-link concentrations as reported by Bachmann et al.[44] One of the biggest challenges in tissue engineering facing the use of hydrogels resides in the ability to resemble the tissues' mechanical and viscoelastic characteristics.[45] Oftentimes, hydrogel-based tissues present weaker mechanical strength than their native counterpart.[46,47] Moreover, the difference in terms of stiffness is a crucial aspect since it can affect the behavior of stem cells, fibroblasts, and other types of cells, thereby affecting the process of tissue repair.[48] Despite the differences in terms of formulations' composition, due to the different crosslinkers and the presence of the RGD peptide, Young's modulus values are comparable to soft gels used in skin tissue engineering (0.5–12 kPa for acellular collagen scaffolds),[49] normally employed to simulate dermal substitutes.

3.2. Ability of norbornene-pullulan hydrogels in sustaining dermal cell culture

Human foreskin Hs-27 fibroblasts, acting as representatives for the skin dermal compartment, were added to the pre-gel mixtures at a density of 5×10^6 cells/mL, to test cell viability and proliferation within N-PLN hydrogels printed with a power of 22 mW. This cell density value was selected to minimize light scattering interference on the photocrosslinking process while still providing good cell–cell communication.[27,50]

Cell viability results for the two formulations tested on days 1, 3–4, and 7 of culture are shown in Figure 3a and b. The cell viability after printing (day 1) was high for both pre-gel formulations: 84% ± 5.5 for *Formulation 1* and 88% ± 0.37 for *Formulation 2*, and viable cells were found throughout the entire thickness of the printed constructs (Figure 3a and b). In addition, after 7 days in culture, fibroblasts remained mainly viable in both formulations, reaching values higher than 74%, which are remarkable compared to the values reported for human dermal fibroblasts within gelatin-based hydrogels (42%).[51] However, when comparing both formulations, we noticed that while the fibroblasts in *Formulation 1* remained visibly roundish during culture, the cells within *Formulation 2*

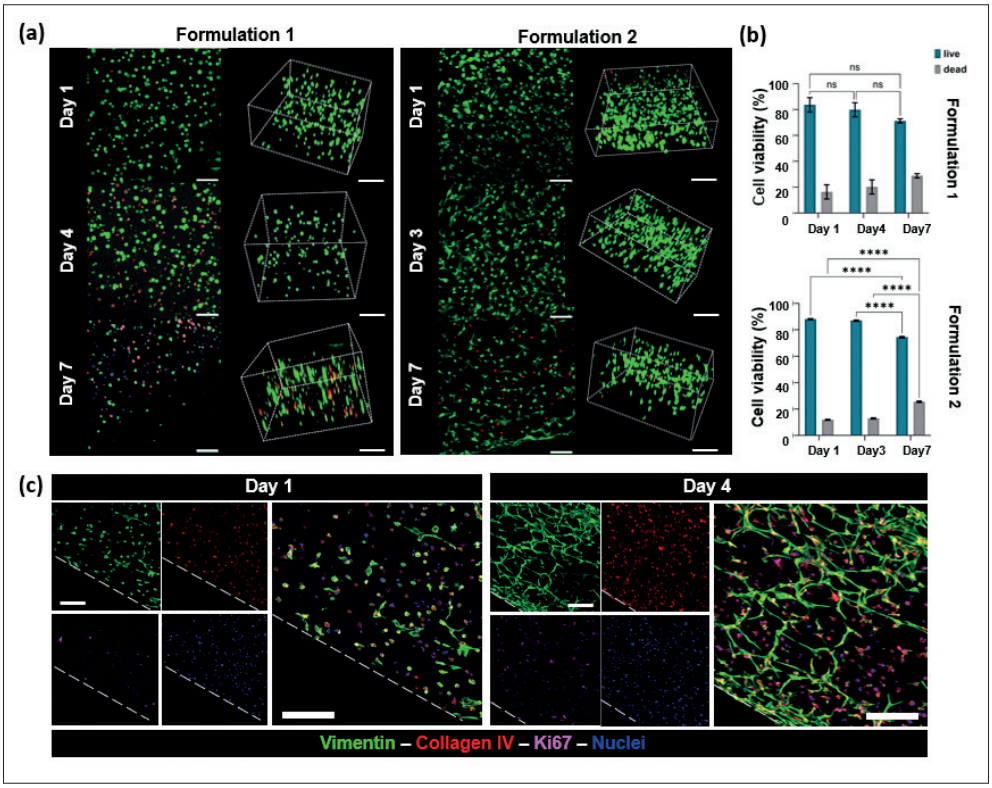

Figure 3. Cell viability and immunofluorescence studies of N-PLN cell-laden hydrogels. **(a)** Top maximum intensity projections and 3D views at days 1, 3–4, and 7 post-Hs-27 encapsulation for *Formulation 1* and *Formulation 2* after live/dead assay. Hydrogels were fabricated with these parameters: power = 22 mW, and beam speed = 0.3 mm/s. Live cells stained in green, and dead cells in red. Scale bars = 100 μm. **(b)** Cell viability quantification based on live/dead staining at days 1, 3–4, and 7 post-Hs-27 encapsulation for both formulations. Percentages of cell viability are expressed as mean ± SEM ($n = 2$); ****$p < 0.0001$. **(c)** Immunostaining of Hs-27 within *Formulation 2* gels at days 1 (left panel) and 4 (right panel) post-Hs-27 encapsulation: vimentin (green), collagen IV (red), Ki67 (magenta), nuclei (blue). Scale bars = 200 μm (left) and 100 μm (right).

developed protrusions already since day 1 and looked spread within the scaffolds (Figure 3a). Overall, these results seem to point out the superiority of *Formulation 2* in sustaining the culture of the fibroblasts, probably due to the addition of RGD peptides in the polymer composition, as these are peptide sequences known for promoting cell–matrix interactions.[52] Thus, we decided to delve into the functionality of cells growing within hydrogels formed from *Formulation 2* by immunostaining. To do this, we examined proliferative cells by staining for Ki67 and determining the presence of collagen IV, which is produced and secreted by the fibroblasts. Cell morphology was imaged after vimentin cytoskeleton staining.

Four days after encapsulation, vimentin was highly expressed in the samples, with the cells totally spread along the hydrogels, especially in the top section (40–50 μm from the top surface) (right panel in Figure 3c). Indeed, in the upper layers, the cells formed interconnections, which were not visible yet in the middle layers (Figure S3, Supporting Information).

Expressed at a low level on day 1 (left panel of Figure 3c), the staining of collagen IV became more conspicuous at the cells' periphery 4 days post-Hs-27 encapsulation, proving the capability of the cells to produce and secrete the protein (right panel of Figure 3c). Moreover, some nuclei showed positive staining for Ki67, therefore demonstrating the proliferative capacity of the cells within hydrogels from *Formulation 2*. Recently, it has been reported that N-PLN hydrogels produced by digital light processing technique do not affect cell metabolic activity nor promote apoptosis.[53] Here, we showed that light-based bioprinting of N-PLN polymers results in hydrogels that not only provide good cell viability but also permit cell proliferation and secretion of relevant extracellular matrix proteins.

The study on these two formulations underscores the importance to strike a balance between mechanical and biological properties of the gels. Although *Formulation 1* could slightly enhance elastic modulus, *Formulation 2* appeared to be a more appropriate choice for supporting

cells and stimulating their growth, due to the presence of a natural-based crosslinker (HA) and RGD peptide.

3.3. Epithelized dermal skin constructs: Toward full-thickness skin

After confirming the suitability of the hydrogels from *Formulation 2* to create a dermal compartment, a co-culture model was developed to produce an epithelized dermal skin construct. Hence, HaCaT cells, which are extensively used in cell culture studies, wound healing, and transplantations,[54–56] were seeded on top of the dermal constructs to mimic the epidermal compartment. To allow for the presence of distinctive apical and basolateral compartments, the constructs were mounted in Transwell® inserts. HaCaT cells are commonly maintained in normal DMEM supplemented with 10% FBS because both contain sufficient calcium to sustain their growth and to induce differentiation,[57] which can also be triggered by the application of specific culture conditions, such as culturing with a combination of different types of cell culture medium both in the apical or basolateral compartments or even in the absence of medium in the apical compartment.

In our model, the seeding time point was established at 3 days post-fibroblast encapsulation, to achieve a proper fibroblast elongation within the matrix so as to sustain the epithelial culture. The same medium was added either into the apical and the basolateral compartments, keeping the samples fully submerged for 7 days (submerged condition). Afterward, ALI conditions, which are necessary to induce keratinocyte differentiation and stratification,[58] were applied to half of the samples, meaning that the medium was removed from the apical compartment and only added into the basolateral one, whereas the other half was kept in submerged conditions. Then, all samples were maintained in co-culture and monitored for an additional 2 weeks (up to 21 days post-HaCaT seeding) (Figure 4a).

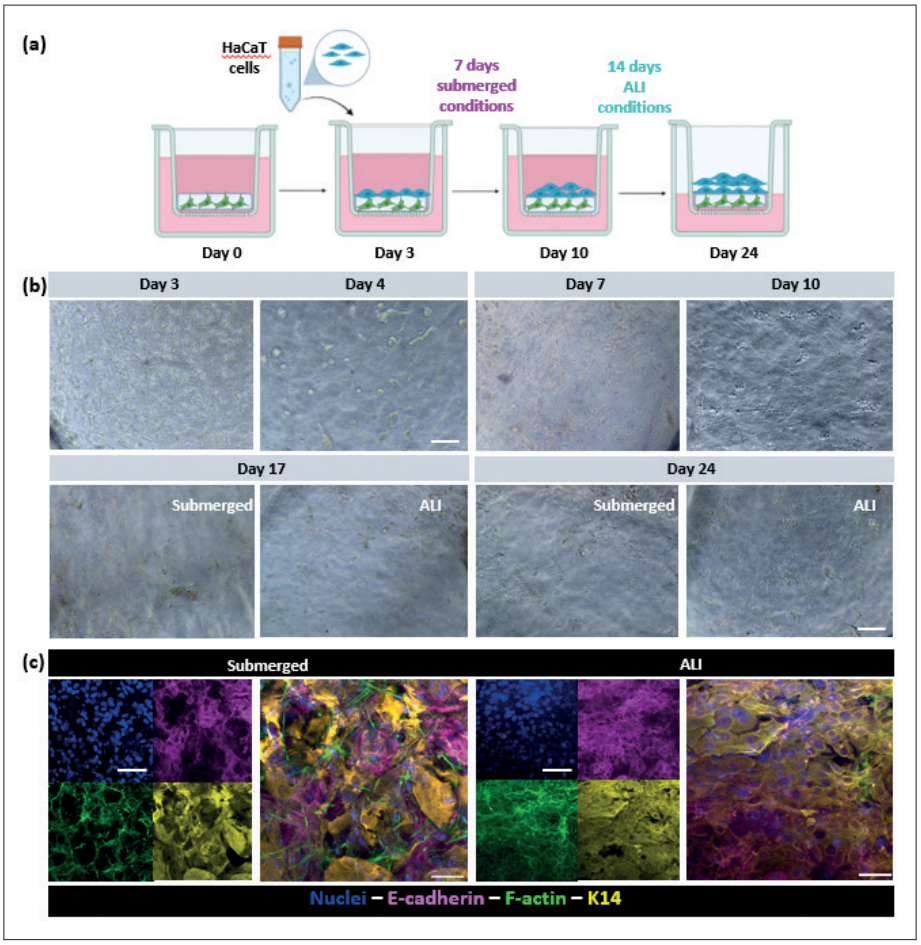

Figure 4. Effect of the culture conditions on the keratinocytes' growth on top of scaffold based on *Formulation 2*. **(a)** Schematic illustration of the co-culture model from day 0 up to day 24 post-fabrication. **(b)** Brightfield pictures of the top view of co-culture constructs (Hs-27 and HaCaT cells) at days 3, 4, 7, and 10 (submerged conditions) and days 17 and 24 (submerged vs. ALI conditions). Scale bars = 200 μm. **(c)** Immunostainings of the main markers for both cellular compartments at 21 days post-HaCaT seeding: E-cadherin (magenta), F-actin (green), and K14 (yellow). Nuclei were stained in blue. Scale bars = 100 μm.

Brightfield inspection of the samples revealed cells fully covering the fibroblast-laden hydrogels by day 10 (Figure 4b). By days 17 and 24 of the experiment, images did not reveal significant differences in terms of cellular morphology between the submerged and ALI culture conditions. In both cases, regions with some clustered cells could be distinguished, which might be related to HaCaT multilayer formation. To elucidate that, the samples were analyzed by immunofluorescence microscopy at day 24 of the experiment (21 days post-HaCaT seeding). Figure 4c shows the dermal fibroblasts (here visualized by the staining of F-actin), which forms a network that appears more compact for the samples cultured in ALI conditions. As specific markers for the keratinocytes, both keratin 14 and E-cadherin were selected (stained in yellow and magenta, respectively) (Figure 4c). Keratin 14 antibody was used to mark the basal layer of non-differentiated epidermis. The keratin 14 signal was visible for samples cultured in both submerged and ALI conditions. However, morphological differences between the submerged and ALI conditions could be observed, with the latter featuring a more evenly distributed signal of keratin 14 (right panel in Figure 4c). Comparable results were found with the E-cadherin signal. This marker was visualized to examine cell–cell contacts and better distinguish the multilayered distribution of the keratinocytes. E-cadherin signal appeared clustered on the scaffolds' surface, especially in the submerged condition, where some uncovered portions were also observed (left panel of Figure 4c). A more uniform and consistent distribution of E-cadherin was found on top of hydrogels cultured in ALI conditions (right panel of Figure 4c), corroborating the importance of the ALI for the growth of human keratinocytes.

Next, the cellular organization and functionality of both skin dermal and epidermal compartments were investigated upon the expression of specific markers for both submerged and ALI conditions. Figure 5a shows representative cross-sections of the resulting hydrogels, where vimentin was stained to highlight the dermal compartment, E-cadherin was chosen as an epidermal marker, and laminin was selected as an extracellular matrix protein marker. Both dermal and epidermal compartments were visibly segregated within the samples. Fibroblasts appeared elongated and uniformly distributed within the bulk of the hydrogels, forming a network, and laying below the epithelial cells for both culture conditions. In addition, the fibroblasts under the ALI condition formed a more entangled mesh as compared to the submerged ones.

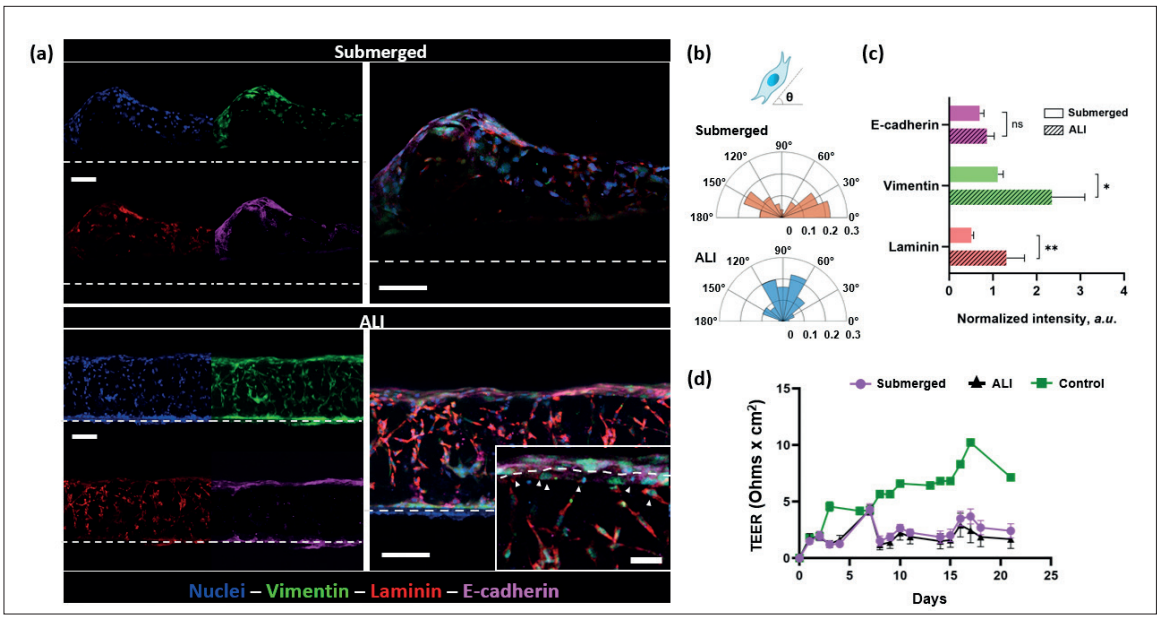

Figure 5. Effect of the co-culture conditions on full-thickness scaffolds based on *Formulation 2*. **(a)** Immunofluorescence staining of the cross-sections of constructs for submerged and ALI conditions 21 days post-HaCaT seeding: nuclei (blue), vimentin (green), laminin (red), and E-cadherin (magenta). Dashed lines refer to the PET membranes (hydrogels' support). Scale bars = 100 μm. Inset shows a detailed view of the interaction of the fibroblasts with the keratinocytes on the basement layer. Scale bar = 25 μm. Quantification of **(b)** the nuclei orientation (normalized from 0 to 1, $n = 2$) and **(c)** the expression of the different markers for both submerged and ALI conditions. Normalized values are presented as mean ± SD ($n = 3$). *$p = 0.0283$; **$p = 0.0495$. **(d)** Transepithelial electrical resistance (TEER) values showing the epithelial monolayer progression on top of conventional Transwell® inserts (green squares: control) and hydrogels with Hs-27 fibroblasts embedded, cultured under submerged conditions (magenta dots) and under ALI conditions (black triangles). Values are expressed as mean ± SEM ($3 \leq n \leq 7$).

Regarding the epidermal compartment, HaCaT cells fully covered the top surface of the hydrogels, as observed with the E-cadherin signal, and no visible differences in terms of cell morphology and compactness were found between both the culture conditions.

The presence of laminin was detected within the cells and at the interface between the epidermal and the dermal compartments. Also, at this interface, fibroblasts were seen elongated and oriented perpendicularly to the surface of the epithelial monolayer, mainly in the case of ALI culture (cell nuclei forming an angle between $60° < \theta < 120°$ with the surface, seen in Figure 5a and b), thus evidencing the close interaction between cells of both compartments. Also, ALI culture conditions appeared as slightly enhancing E-cadherin signal (Figure 5c), which can be correlated with the keratin 14 signal (Figure 4c), and enhancing the vimentin and laminin signals, which were 2.6- and 2.1-fold higher, respectively (Figure 5c).

Subsequently, we assessed the barrier function of the epithelial monolayer formed by measuring the TEER along culture time (Figure 5d). Samples with HaCaT cells seeded on hard porous membranes were used as controls. TEER values measured for the hydrogel samples were lower than values measured in controls (~2.5 $\Omega \cdot cm^2$ vs. ~10 $\Omega \cdot cm^2$) but in line with other studies that also employed HaCaT cells.[18,59,60] No differences in TEER values were found for samples cultured under submerged or ALI conditions. Remarkably, no visible shrinkage and/or gels' degradation were detected even at long-term cultures, making the N-PLN formulation well-suited for standard Transwell® inserts, where TEER and/or permeability tests can be performed in a routine manner.

These data indicated that ALI culture condition might be advantageous for long culture periods. Given this, we proceeded to evaluate the specific benefits of ALI culture conditions for both the epithelial and the dermal compartments by quantifying specific markers. In the epithelial compartment, the levels of keratin 14 and E-cadherin markers under ALI culture condition did not show statistically significant differences compared to those under submerged condition (Figure 6b).

However, the images of the samples' cross-sections show varied spatial distribution of markers. Keratinocytes did not form a continuous monolayer in submerged condition, whereas marker signals for fibronectin and collagen IV appeared denser and more homogeneous in samples cultured under ALI condition. Moreover, a better interconnection between the epithelial monolayer and the dermis was observed in samples under ALI conditions (bottom panel of Figure 6a).

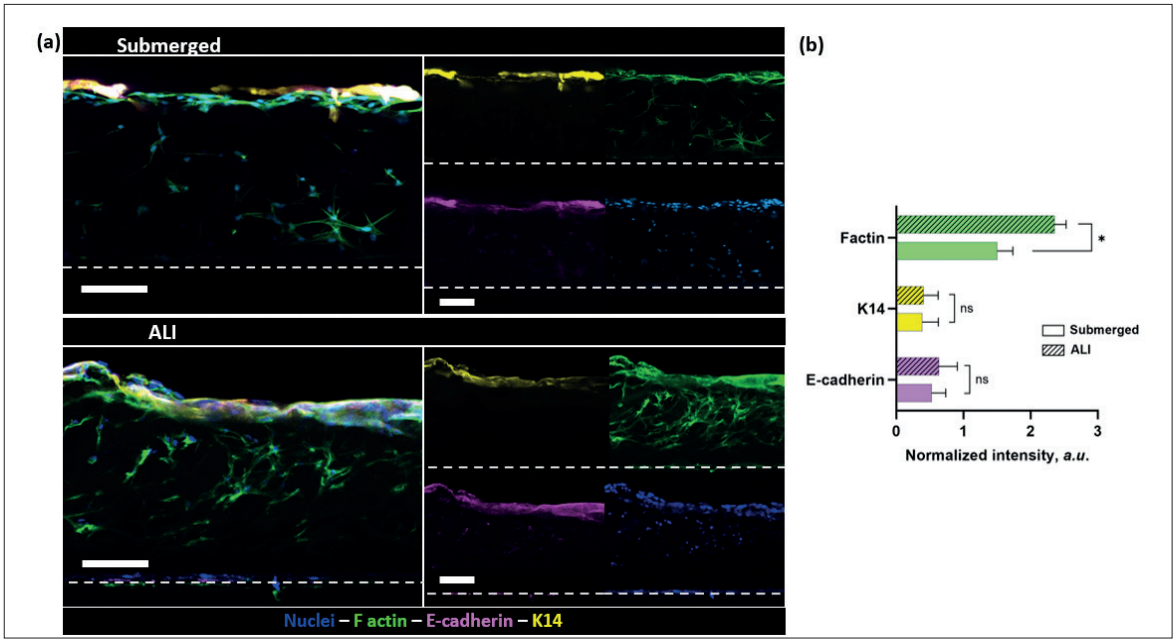

Figure 6. Effect of the co-culture conditions on the epidermal compartment in hydrogels based on *Formulation 2.* (a) Immunofluorescence staining of main epidermal markers in the cross-sections of constructs for both submerged (top panel) and ALI (lower panel) culture conditions 21 days post-HaCaT seeding: E-cadherin (magenta), and keratin 14 (yellow). The stained F-actin (green) indicated both the fibroblast network in the dermal compartment and the keratinocytes. Nuclei were stained in blue. Dashed lines refer to the PET membranes (hydrogels' support). Scale bars = 100 μm. (b) Quantification of the expression of the different markers for both submerged and ALI conditions. Normalized values are expressed as mean ± SD ($n = 3$). *$p = 0.0381$.

Regarding the dermal compartment, in addition to the higher connectivity of the fibroblasts (Figures 5a and 7b), ALI cultures also exhibited increased collagen IV and fibronectin signals. Collagen IV appeared segregated on the surface of the dermal compartment (interface between the dermis and epidermis), resembling the basement membrane found *in vivo*. Meanwhile, fibronectin fibrils, which play a crucial role in the formation of extracellular matrix and the re-epithelialization,[61] were also found within the hydrogel and on the surface (Figure 7a and b). Taken together, these results corroborated the superiority of ALI conditions for the formation of epithelized dermal skin constructs.

Epidermis models such as Episkin™, SkinEthic®, and EpiDerm®[62–64], as well as full-thickness human skin such as GraftSkin®, EpiDermFT®, and Pheninon®,[64,65] are available on the market, but they are very costly for *in vitro* testing and not easy to modify with specific appendages or to tailor to disease conditions. In this context, the use of 3D bioprinting holds great promise, as demonstrated by the use of collagen and chitosan derivatives as bioinks.[66,67] Recently, N-PLN gels have gained popularity, highlighting the potential of these photocrosslinkable materials;[53] however, biological studies surrounding the specific applications of N-PLN are scarce. In the current study, we demonstrated the potential of a novel strategy combining an easy and low-cost 3D bioprinting system with a PLN-based bioink to produce skin-like models. Overall, the results presented here highlight the potential of these novel thiol-ene inks to compete in the bioinks panorama. Given that new affordable approaches are in great demand among the cosmetic and pharmaceutical companies, as well as in toxicological research landscape, we believe that novel bioinks such as N-PLN might find a place serving the relevant purposes.

4. Conclusion

This study presents a promising strategy to develop an epithelized dermal human skin model by exploiting a custom-made 3D light-based bioprinting system and novel N-PLN polymers. Upon fast exposure with a low dose of visible light, the hydrogels formed possess the proper physicochemical properties to sustain excellent cell viability, proliferation, matrix protein secretion and elongation, which are essential for the formation of cellular networks. In addition, the fibroblast-laden hydrogels can sustain the culture of keratinocytes, thus paving the way for the formation of epithelized dermal constructs. Evidenced

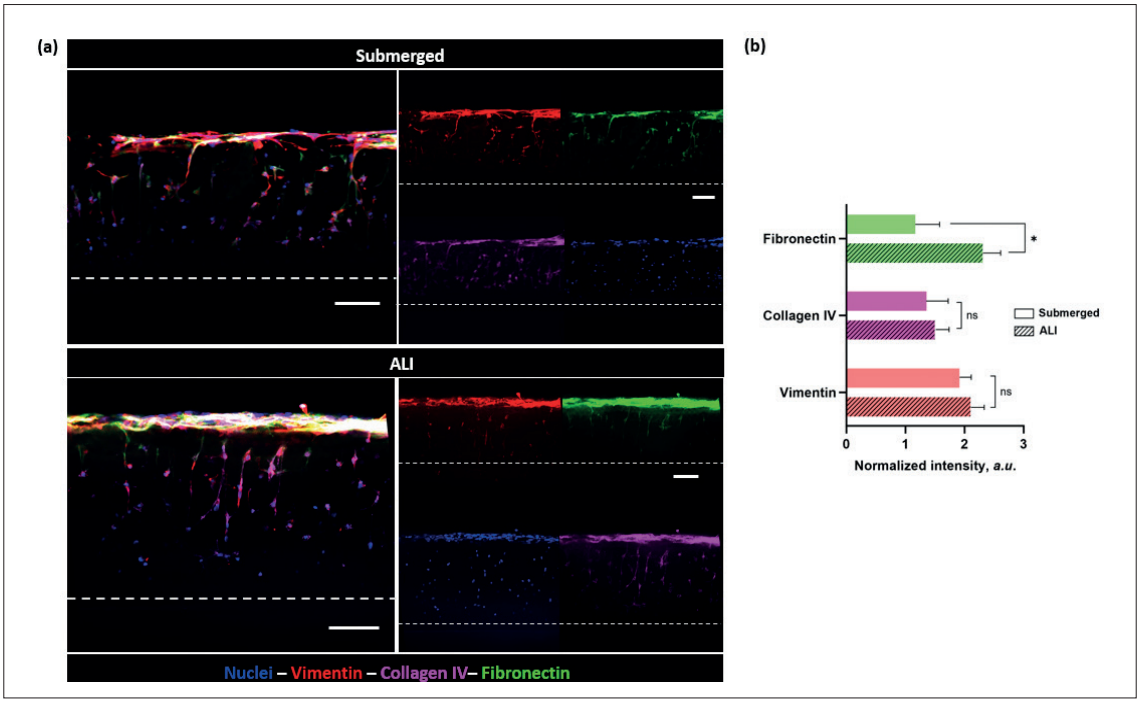

Figure 7. Effect of the co-culture conditions on the dermal compartment of scaffolds based on *Formulation 2*. **(a)** Immunofluorescence staining of main dermal markers in the cross-sections of constructs for both submerged (top panel) and ALI (lower panel) culture conditions 21 days post-HaCaT seeding: vimentin (red), collagen IV (magenta), and fibronectin (green). Nuclei were stained in blue. Dashed lines refer to the PET membranes (hydrogels' support). Scale bars = 100 µm. **(b)** Quantification of the expression of the different markers for both submerged and ALI conditions. Normalized values are expressed as mean ± SD ($n = 3$). *$p = 0.0311$.

by the expression of cellular markers, these constructs exhibit *in vivo*-like cell organization, featuring dermis and epidermis, and boast barrier characteristics as confirmed by the TEER measurements. Cellular distribution and, especially, epithelial-dermal cell interaction, can be promoted by culturing the constructs under ALI condition. Altogether, this approach represents an alternative method to develop ready-to-use skin models in an easily, fast, reproducible, and cost-affordable manner, which might be particularly beneficial for pre-clinical assays in cosmetic and pharmaceutical research.

Acknowledgments

Not applicable.

Funding

This work was supported by the European Union's Horizon Europe Research and Innovation Programme (B-BRIGHTER project, grant agreement no. 101057894), the Department of Research and Universities of the Generalitat de Catalunya (2021 SGR 01495), and the CERCA Programme of the Generalitat de Catalunya. N.T. acknowledges the Spanish Ministry of Science and Innovation (MCIN) for her Juan de la Cierva grant (IJC2019-040289-I, MCIN/AEI/ 10.13039/501100011033). Views and opinions expressed in this work are however those of the author(s) only and do not necessarily reflect those of the European Union. Neither the European Union nor the granting authority can be held responsible for them.

Conflict of interest

The authors declare no conflicts of interest.

Author contributions

Conceptualization: Núria Torras, Elena Martínez
Formal analysis: Angela Cirulli, Livia Neves Borgheti-Cardoso, Núria Torras
Investigation: Angela Cirulli, Livia Neves Borgheti-Cardoso
Methodology: Núria Torras, Elena Martínez, Angela Cirulli
Supervision: Núria Torras, Elena Martínez
Writing – original draft: Angela Cirulli
Writing – review & editing: Angela Cirulli, Livia Neves Borgheti-Cardoso, Núria Torras, Elena Martínez
All authors have read and approved the manuscript.

Ethics approval and consent to participate

Not applicable.

Consent for publication

Not applicable.

Availability of data

Data are available from the corresponding author upon reasonable request.

References

1. Moniz T, Costa Lima SA, Reis S. Human skin models: from healthy to disease-mimetic systems; characteristics and applications. *Br J Pharmacol*. 2020;177(19):4314-4329. doi: 10.1111/bph.15184

2. Dearman BL, Boyce ST, Greenwood JE. Advances in skin tissue bioengineering and the challenges of clinical translation. *Front Surg*. 2021;8:640879. doi: 10.3389/fsurg.2021.640879

3. Shores JT, Gabriel A, Gupta S. Skin substitutes and alternatives. *Adv Skin Wound Care*. 2007;20(9):493-508. doi: 10.1097/01.ASW.0000288217.83128.f3

4. Manon-Jensen T, Kjeld NG, Karsdal MA. Collagen-mediated hemostasis. *J Thromb Haemost*. 2016;14(3):438-448. doi: 10.1111/jth.13249

5. Sorushanova A, Delgado LM, Wu Z, et al. The collagen suprafamily: from biosynthesis to advanced biomaterial development. *Adv Mater*. 2019;31(1):e1801651. doi: 10.1002/adma.201801651

6. Eming SA, Martin P, Tomic-Canic M. Wound repair and regeneration: Mechanisms, signaling, and translation. *Sci Transl Med*. 2014;6(265):265sr6. doi: 10.1126/scitranslmed.3009337

7. Silvipriya KS, Krishna Kumar K, Bhat AR, Dinesh Kumar B, John A, Lakshmanan P. Collagen: animal sources and biomedical application. *J Appl Pharm Sci*. 2015;5(3): 123-127. doi: 10.7324/JAPS.2015.50322

8. Schmidt FF, Nowakowski S, Kluger PJ. Improvement of a three-layered in vitro skin model for topical application of irritating substances. *Front Bioeng Biotechnol*. 2020;8(May):1-11. doi: 10.3389/fbioe.2020.00388

9. Wang H. A review of the effects of collagen treatment in clinical studies. *Polymers (Basel)*. 2021;13(22):3868. doi: 10.3390/polym13223868

10. Keefe J, Wauk L, Chu S, DeLustro F. Clinical use of injectable bovine collagen: a decade of experience. *Clin Mater*. 1992;9(3-4):155-162. doi: 10.1016/0267-6605(92)90095-b

11. Bacakova M, Pajorova J, Broz A, et al. A two-layer skin construct consisting of a collagen hydrogel reinforced by a fibrin-coated polylactide nanofibrous membrane. *Int J Nanomedicine*. 2019;14:5033-5050. doi: 10.2147/IJN.S200782

12. Ackermann K, Lombardi Borgia S, Korting HC, Mewes KR, Schäfer-Korting M. The Phenion® full-thickness skin model

for percutaneous absorption testing. *Skin Pharmacol Physiol*. 2010;23(2):105-112.
doi: 10.1159/000265681

13. Zhang Y, Wang Y, Li Y, et al. Application of collagen-based hydrogel in skin wound healing. *Gels*. 2023;9(3):185.
doi: 10.3390/gels9030185

14. Zhu J, Marchant RE. Design properties of hydrogel tissue-engineering scaffolds. *Expert Rev Med Devices*. 2011;8(5):607-626.
doi: 10.1586/erd.11.27

15. Sun M, Sun X, Wang Z, Guo S, Yu G, Yang H. Synthesis and properties of gelatin methacryloyl (GelMA) hydrogels and their recent applications in load-bearing tissue. *Polymers (Basel)*. 2018;10(11):1290.
doi: 10.3390/polym10111290

16. Yegappan R, Selvaprithiviraj V, Amirthalingam S, Jayakumar R. Carrageenan based hydrogels for drug delivery, tissue engineering and wound healing. *Carbohydr Polym*. 2018;198:385-400.
doi: 10.1016/j.carbpol.2018.06.086

17. Park D, Kim Y, Kim H, et al. Hyaluronic acid promotes angiogenesis by inducing RHAMM-TGFβ receptor interaction via CD44-PKCδ. *Mol Cells*. 2012;33(6):563-574.
doi: 10.1007/s10059-012-2294-1

18. Toole BP. Hyaluronan: from extracellular glue to pericellular cue. *Nat Rev Cancer*. 2004;4(7):528-539.
doi: 10.1038/nrc1391

19. Gobi R, Ravichandiran P, Babu RS, Yoo DJ. Biopolymer and synthetic polymer-based nanocomposites in wound dressing applications: a review. *Polymers (Basel)*. 2021;13(12):1962.
doi: 10.3390/polym13121962

20. Li R, Tomasula P, de Sousa AMM, et al. Electrospinning pullulan fibers from salt solutions. *Polymers (Basel)*. 2017;9(1):32.
doi: 10.3390/polym9010032

21. Leathers TD. Biotechnological production and applications of pullulan. *Appl Microbiol Biotechnol*. 2003;62(5-6): 468-473.
doi: 10.1007/s00253-003-1386-4

22. Cheng N, Jeschke MG, Sheikholeslam M, Datu A, Oh HH, Amini-Nik S. Promotion of dermal regeneration using pullulan/gelatin porous skin substitute. *J Tissue Eng Regen Med*. 2019;13(11):1965-1977.
doi: 10.1002/term.2946

23. Wang Y, Yuan X, Yao B, Zhu S, Zhu P, Huang S. Tailoring bioinks of extrusion-based bioprinting for cutaneous wound healing. *Bioact Mater*. 2022;17:178-194.
doi: 10.1016/j.bioactmat.2022.01.024

24. Antezana PE, Municoy S, Álvarez-Echazú MI, et al. The 3D bioprinted scaffolds for wound healing. *Pharmaceutics*. 2022;14(2):464.
doi: 10.3390/pharmaceutics14020464

25. Zhang Q, Bei HP, Zhao M, Dong Z, Zhao X. Shedding light on 3D printing: Printing photo-crosslinkable constructs for tissue engineering. *Biomaterials*. 2022;286:121566.
doi: 10.1016/j.biomaterials.2022.121566

26. Yu C, Schimelman J, Wang P, et al. Photopolymerizable biomaterials and light-based 3D printing strategies for biomedical applications. *Chem Rev*. 2020;120(19): 10695-10743.
doi: 10.1021/acs.chemrev.9b00810

27. Torras N, Zabalo J, Abril E, Carré A, García-Díaz M, Martínez E. A bioprinted 3D gut model with crypt-villus structures to mimic the intestinal epithelial-stromal microenvironment. *Biomater Adv*. 2023;153:213534.
doi: 10.1016/j.bioadv.2023.213534

28. Lin CC, Raza A, Shih H. PEG hydrogels formed by thiol-ene photo-click chemistry and their effect on the formation and recovery of insulin-secreting cell spheroids. *Biomaterials*. 2011;32(36):9685-9695.
doi: 10.1016/j.biomaterials.2011.08.083

29. McCall JD, Anseth KS. Thiol–ene photopolymerizations provide a facile method to encapsulate proteins and maintain their bioactivity. *Biomacromolecules*. 2012;13(8):2410-2417.
doi: 10.1021/bm300671s

30. Fairbanks BD, Schwartz MP, Halevi AE. A Versatile Synthetic Extracellular Matrix Mimic via Thio-Norbornene Photopolymerization. *Adv Mater*. 2009;21(48):5005-5010.
doi: 10.1002/adma.200901808

31. Lin CC, Ki CS, Shih H. Thiol-norbornene photoclick hydrogels for tissue engineering applications. *J Appl Polym Sci*. 2015;132(8):1-11.
doi: 10.1002/app.41563

32. Van Hoorick J, Dobos A, Markovic M, et al. Thiol-norbornene gelatin hydrogels: Influence of thiolated crosslinker on network properties and high definition 3D printing. *Biofabrication*. 2020;13(1): 1-22.
doi: 10.1088/1758-5090/abc95f

33. Anseth KS, Bowman CN, Brannon-Peppas L. Mechanical properties of hydrogels and their experimental determination. *Biomaterials*. 1996;17(17):1647-1657.
doi: 10.1016/0142-9612(96)87644-7

34. Vila A, Torras N, Castaño AG, et al. Hydrogel co-networks of gelatine methacrylate and poly(ethylene glycol) diacrylate sustain 3D functional in vitro models of intestinal mucosa. *Biofabrication*. 2020;12(2):025008.
doi: 10.1088/1758-5090/ab5f50

35. Nguyen AL, Grothe S, Luong JHT. Applications of pullulan in aqueous two-phase systems for enzyme production, purification and utilization. *Appl Microbiol Biotechnol*. 1988:27;341-346.
doi: 10.1007/BF00251765

36. Singh RS, Kaur N, Singh D, Kennedy JF. Investigating aqueous phase separation of pullulan from Aureobasidium

pullulans and its characterization. *Carbohydr Polym*. 2019;223:115103.
doi: 10.1016/j.carbpol.2019.115103

37. Knight CG, Willenbrock F, Murphy G. A novel coumarin-labelled peptide for sensitive continuous assays of the matrix metalloproteinases. *FEBS Lett*. 1992;296(3):263-266.
doi: 10.1016/0014-5793(92)80300-6

38. Holback H, Yeo Y, Park K. Hydrogel swelling behavior and its biomedical applications. *Biomed Hydrogels*. 2011;1:3-24.
doi: 10.1533/9780857091383.1.3

39. Chyzy A, Plonska-Brzezinska ME. Hydrogel properties and their impact on regenerative medicine and tissue engineering. *Molecules*. 2020;25(24):5795.
doi: 10.3390/molecules25245795

40. Suhaeri M, Noh MH, Moon JH, et al. Novel skin patch combining human fibroblast-derived matrix and ciprofloxacin for infected wound healing. *Theranostics*. 2018;8(18):5025-5038.
doi: 10.7150/thno.26837

41. Wu DQ, Zhu J, Han H, et al. Synthesis and characterization of arginine-NIPAAm hybrid hydrogel as wound dressing: in vitro and in vivo study. *Acta Biomater*. 2018;65:305-316.
doi: 10.1016/j.actbio.2017.08.048

42. Peppas NA, Bures P, Leobandung W, Ichikawa H. Hydrogels in pharmaceutical formulations. *Eur J Pharm Biopharm*. 2000;50(1):27-46.
doi: 10.1016/S0939-6411(00)00090-4

43. Lai VK, Nedrelow DS, Lake SP, et al. Swelling of collagen-hyaluronic acid co-gels: an in vitro residual stress model. *Ann Biomed Eng*. 2016;44(10):2984-2993.
doi: 10.1007/s10439-016-1636-0

44. Bachmann B, Spitz S, Schädl B, et al. Stiffness matters: fine-tuned hydrogel elasticity alters chondrogenic redifferentiation. *Front Bioeng Biotechnol*. 2020;8:373.
doi: 10.3389/fbioe.2020.00373

45. Ahearne M, Yang Y, El Haj AJ, Then KY, Liu KK. Characterizing the viscoelastic properties of thin hydrogel-based constructs for tissue engineering applications. *J R Soc Interface*. 2005;2(5):455-463.
doi: 10.1098/rsif.2005.0065

46. Orwin EJ, Borene ML, Hubel A. Biomechanical and optical characteristics of a corneal stromal equivalent. *J Biomech Eng*. 2003;125(4):439-444.
doi: 10.1115/1.1589773

47. Awad HA, Quinn Wickham M, Leddy HA, Gimble JM, Guilak F. Chondrogenic differentiation of adipose-derived adult stem cells in agarose, alginate, and gelatin scaffolds. *Biomaterials*. 2004;25(16):3211-3222.
doi: 10.1016/j.biomaterials.2003.10.045

48. R. Ibañez RI, do Amaral RJFC, Reis RL, Marques AP, Murphy CM, O'Brien FJ. 3D-printed gelatin methacrylate scaffolds with controlled architecture and stiffness modulate the fibroblast phenotype towards dermal regeneration. *Polymers (Basel)*. 2021;13(15):2510.
doi: 10.3390/polym13152510

49. Raub CB, Putnam AJ, Tromberg BJ, George SC. Predicting bulk mechanical properties of cellularized collagen gels using multiphoton microscopy. *Acta Biomater*. 2010;6(12):4657-4665.
doi: 10.1016/j.actbio.2010.07.004

50. Weng T, Zhang W, Xia Y, et al. 3D bioprinting for skin tissue engineering: current status and perspectives. *J Tissue Eng*. 2021;12:204173142110285.
doi: 10.1177/20417314211028574

51. Tahri S, Maarof M, Masri S, Che Man R, Masmoudi H, Fauzi MB. Human epidermal keratinocytes and human dermal fibroblasts interactions seeded on gelatin hydrogel for future application in skin in vitro 3-dimensional model. *Front Bioeng Biotechnol*. 2023;11:1200618.
doi: 10.3389/fbioe.2023.1200618

52. Bott K, Upton Z, Schrobback K, et al. The effect of matrix characteristics on fibroblast proliferation in 3D gels. *Biomaterials*. 2010;31(32):8454-8464.
doi: 10.1016/j.biomaterials.2010.07.046

53. Feng Z, Li J, Zhou D, Song H, Lv J, Bai W. A novel photocurable pullulan-based bioink for digital light processing 3D printing. *Int J Bioprint*. 2022;9(2):104-117.
doi: 10.18063/ijb.v9i2.657

54. Boelsma E, Verhoeven MCH, Ponec M. Reconstruction of a human skin equivalent using a spontaneously transformed keratinocyte cell line (HaCaT). *J Invest Dermatol*. 1999;112(4):489-498.
doi: 10.1046/j.1523-1747.1999.00545.x

55. Schoop VM, Fusenig NE, Mirancea N. Epidermal organization and differentiation of HaCaT keratinocytes in organotypic coculture with human dermal fibroblasts. *J Invest Dermatol*. 1999;112(3):343-353.
doi: 10.1046/j.1523-1747.1999.00524.x

56. Maas-Szabowski N, Stärker A, Fusenig NE. Epidermal tissue regeneration and stromal interaction in HaCaT cells is initiated by TGF-α. *J Cell Sci*. 2003;116(Pt 14):2937-2948.
doi: 10.1242/jcs.00474

57. Wilson VG. Growth and differentiation of HaCaT keratinocytes. *Methods Mol Biol*. 2014;1195:33-41.
doi: 10.1007/7651_2013_42

58. Zhao X, Lang Q, Yildirimer L, et al. Photocrosslinkable gelatin hydrogel for epidermal tissue engineering. *Adv Healthc Mater*. 2016;5(1):108-118.
doi: 10.1002/adhm.201500005

59. Meyle J, Guttig K, Rascher G, Wolburg H. Transepithelial electrical resistance and tight junctions of human gingival keratinocytes. *J Periodontal Res*. 1999;34(4):214-222.
doi: 10.1111/j.1600-0765.1999.tb02244.x

60. Le Ferrec E, Chesne C, Artusson P, et al. In vitro models of the intestinal barrier: the report and recommendations of ECVAM workshop 46. Altern Lab Anim. 2001;29(6): 649-668.
doi: 10.1177/026119290102900604

61. Lenselink EA. Role of fibronectin in normal wound healing. *Int Wound J*. 2015;12(3):313-316.
doi: 10.1111/iwj.12109

62. Flaten GE, Palac Z, Engesland A, Filipović-Grčić J, Vanić Ž, Škalko-Basnet N. In vitro skin models as a tool in optimization of drug formulation. *Eur J Pharm Sci*. 2015;75:10-24.
doi: 10.1016/j.ejps.2015.02.018

63. Randall MJ, Jüngel A, Rimann M, Wuertz-Kozak K. Advances in the biofabrication of 3D skin in vitro: healthy and pathological models. *Front Bioeng Biotechnol*. 2018;6:154.
doi: 10.3389/fbioe.2018.00154

64. Yun YE, Jung YJ, Choi YJ, Choi JS, Cho YW. Artificial skin models for animal-free testing. *J Pharm Investig*. 2018;48(2):215-223.
doi: 10.1007/s40005-018-0389-1

65. Abd E, Yousef SA, Pastore MN, et al. Skin models for the testing of transdermal drugs. *Clin Pharmacol*. 2016;8: 163-176.
doi: 10.2147/CPAA.S64788

66. Cirulli A, Neves Borgheti-Cardoso L, Torras N, García-Díaz M, Martínez E. Hydrogels as tissue barriers. In: Oliveira JM, Silva-Correia J, Reis RL, eds. *Hydrogels for Tissue Engineering and Regenerative Medicine*. Elsevier; 2024:433-466.
doi: 10.1016/B978-0-12-823948-3.00017-8

67. Mawazi SM, Kumar M, Ahmad N, Ge Y, Mahmood S. Recent applications of chitosan and its derivatives in antibacterial, anticancer, wound healing, and tissue engineering fields. *Polymers (Basel)*. 2024;16(10):1351.
doi: 10.3390/polym16101351